Combustion and Flame 258 (2023) 113043

Contents lists available at ScienceDirect

Combustion and Flame

journal homepage: www.elsevier.com/locate/combustflame

A simple method for the quantitative assessment of soot production rate

Kevin Gleason[#], Alessandro Gomez[*]

Department of Mechanical Engineering and Materials Science, Yale University, 9 Hillhouse Avenue, New Haven, CT 06520-8286, USA

ARTICLE INFO

Article history:
Received 4 May 2023
Revised 22 August 2023
Accepted 23 August 2023
Available online 8 September 2023

Keywords:
Soot
Counterflow
Diffusion flame
Aliphatics

ABSTRACT

Sooting tendency has been characterized with various empirical approaches such as smoke height and Threshold Sooting Index (TSI), that can be regarded as qualitative, as well as Yield Sooting Index (YSI), that is semiquantitative since it relies on the measurements of at least the peak soot volume fraction in the flame. All these techniques have the convenience of being easy to implement and of relying on inexpensive equipment. In the present work we present a comparatively easy but *quantitative* alternative to determine the soot production rate in counterflow flames. The approach is rooted in the use of: a) soot volume fraction measurements by pyrometry, b) the well established one-dimensional computational modeling of such flames for the determination of temperature and velocity profiles and c) the use of the soot governing equation. The technique is applied to several aliphatics, including methane, propane, ethylene, propene and acetylene. Soot production rate per unit flame area for the tested aliphatics ranges between 10^{-4} and 10^{-7} g/(cm^{2}s) and, when normalized with respect to the carbon flux, between 10^{-5} and 10^{-2}. On a logarithmic scale it correlates linealry with the peak temperature for all fuels. Soot yield scales as alkanes< alkenes < alkynes, with acetylene showing the highest sooting tendency even in flames at relatively low temperatures.

1. Introduction

Sooting tendency has been characterized qualitatively with various empirical approaches. Smoke point measurements were established nearly seventy years with a measurement of the minimum height at which a flame begins to issue a streak of black smoke. It is assessed using either standardizing equipment such as an ASTM smoke point lamp [1] or axisymmetric laminar diffusion flames. The Threshold Sooting Index (TSI) was introduced as an algebraic correlation of the fuel molecular weight and flame height at the smoke point, but included apparatus-dependent constants. The original definition for single fuel was extended to mixtures of fuels, practical fuels and their surrogates [2,3]. An improved normalization method of the smoke point was introduced in [4] and evaluated for many hydrocarbons to assess the effects of fuel type. The Yield Sooting Index (YSI) converts maximum soot concentration in a doped methane/air flame into another index describing the fuel propensity to soot by relying either on laser-induced incandescence [5] or two-color pyrometry [6] for the quantification of the peak soot volume fraction. YSI has been used to classify hundreds of compounds and has been recently correlated with the smoke point height [7]. Of these techniques, the smoke point height and its derivative, TSI, are qualitative and consist in a height measurement accounting for both production in the core of the flame and oxidation in its upper part [8], which is dependent on the flame configuration. YSI correlates better with soot production since it relies on the measurement of the maximum soot concentration before oxidation sets in and, as such, it can be considered semiquantitative. All of them have the convenience of being easy to implement and of relying on simple, inexpensive equipment. As a result, they are adopted often to make comparisons of sooting tendencies of various fuels, without the need for an elaborate infrastructure to pursue quantitative soot research.

In the present work we introduce a comparatively easy but *quantitative* alternative based on three components: a) a counterflow burner to enable the aerodynamic anchoring of one-dimensional diffusion flames, b) one-dimensional modeling of the flames and c) soot volume fraction measurements by pyrometry. The counterflow flame has been a benchmark for laminar flame studies and has been used extensively in soot studies [9]. Its one-dimensional nature facilitates the use of computational modeling with detailed chemical kinetics that has become a commodity in combustion research. Commercial and open-source codes

* Corresponding author.
E-mail address: Alessandro.Gomez@yale.edu (A. Gomez).
Current address: General Electric-Aerospace, 1 Neumann Way, Cincinnati, OH 45215, USA.

https://doi.org/10.1016/j.combustflame.2023.113043
0010-2180/

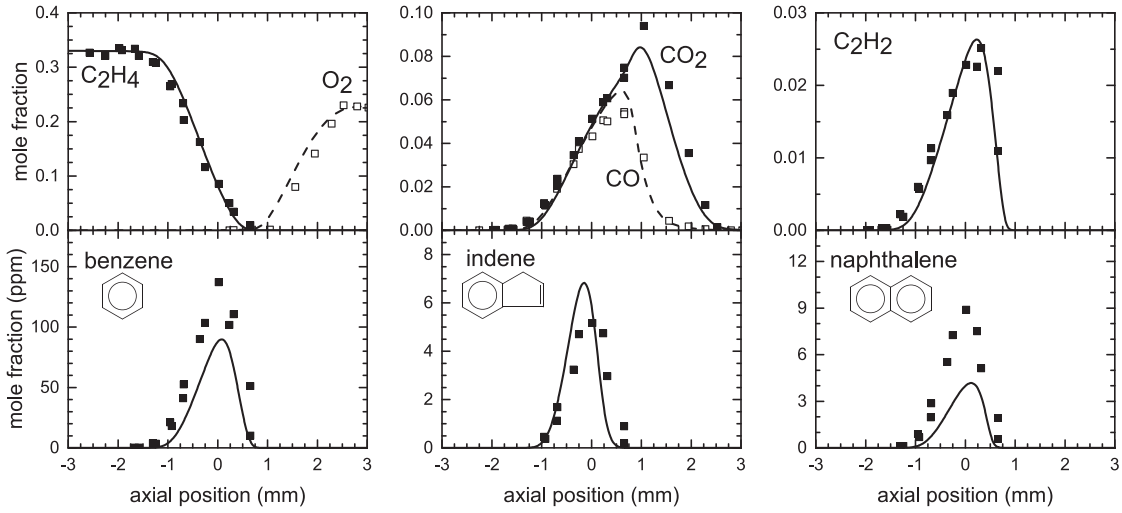

Fig. 1. Profiles of mole fraction of reactants, major products and key aromatics.

(e.g., [10,11]) enable even researchers with modest computational background to make use of these codes for research purposes. The main uncertainty lies in the chemical kinetic mechanism that is well established and validated for aliphatic fuels but becomes progressively less reliable for aromatics, practical fuel surrogates and soot. Still, certain aspects of the model such as the velocity and temperature field are computed reliably in all cases so long as energy losses by radiation are either negligible or properly accounted for [12]. As to the soot field, computational predictions are semi-quantitative and typically within one order of magnitude of experimental measurements, unless special efforts are made to tweak the code by using experimental measurements in the validation process. Pyrometry does not require any laser source and can be realized using a spectrally well-characterized and inexpensive digital camera [12,13]. As a result, it is within experimental reach of virtually all combustion laboratories, without requiring more expensive laser instrumentation and more challenging training. The measurement is of the same type as the one used in the determination of the YSI [6].

Using the computational model to obtain velocity and temperature profiles and pyrometry to obtain soot volume fraction profiles enables the computation of the soot production rate from the soot governing equation, so long as radiative heat losses are estimated to have negligible effects on the temperature profile in the soot forming region [12].

As a demonstration of the method, we present soot production rates of several aliphatics, such as methane, propane, ethylene, propene and acetylene, as well as their temperature dependence for a total of 26 flames.

1.1. Examples of validation of the computational model

As reported in [14], to obtain profiles of concentrations of reactants, intermediates and products, as well as temperature, soot volume fraction and dispersion exponent measurements, we: a) inserted a sampling probe connected to the injection port of a gas chromatograph/mass spectrometer system to quantify H_2, O_2, N_2, CO, CO_2, and hydrocarbons up to three-ring PAH (190 amu); b) used a silica coated R-type thermocouple and performed standard corrections for radiative losses through a convective-radiative energy balance; and c) applied pyrometry using a camera with a well characterized spectral response (400nm-700 nm). Details of the experimental approach are provided ibid. The flames investigated are laminar and very stable.

Profiles of reactants, major combustion products, acetylene, as a critical species in soot surface growth, and some key aromatics are reproduced from Ref. [14,15] in Fig. 1 to inform on the nature of the flame and set the stage for further data analysis in the present article. The abscissa in all plots is the distance from the gas stagnation plane (GSP) with the fuel (oxidizer) stream on the left (right), represented by negative (positive) values of the axial coordinate. Results in Fig. 1 confirms that the model predictions agree with experimental results very well and provides evidence of the successful validation of the model. As further evidence, Fig. 2 shows experimental and computational temperature profiles of the same flame and of another sooting flame of the same fuel, but with a different stoichiometry. Error bars in the reported temperature measurements represent the 95% confidence of the overall uncertainty in the measurements, including the uncertainty in measured position of the thermocouple junction and measured temperature; general uncertainty analysis is applied to assess the error propagation. Also in this case the model predictions and measurements agree very well, especially in the region where soot is present for value of the abscissa ranging from −0.2 mm to 0.8 mm.

The implication of the demonstrated validation in these figures is twofold: if both species and temperature profiles are in agreement, the velocity profiles will also be, which allows us to sidestep the challenge of performing measurement in a low velocity field with significant thermophoretic effects; furthermore, since the chemical kinetics of other aliphatic fuels has been validated in other contexts, we expect that the model predictions of velocity and temperature field are reliable also for such fuels so long as radiative effects are negligible.

2. Methods

2.1. Burner geometry and flame selection

The burner consists of two identical converging nozzles oriented in counterflow configuration [16]. The internal diameter of each nozzle is 6.35 mm and the nozzles are separated by 10 mm. Both nozzles are surrounded by a nitrogen shroud to shield the flame from external disturbances. The counterflow configuration provides a one-dimensional flow field in the vicinity of the burner axis, as confirmed by digital camera photographs showing a locally flat flame. Flames are perturbed by varying the inert concentration in the feed streams to span a range of peak temperatures, but keeping constant the stoichiometric mixture fraction

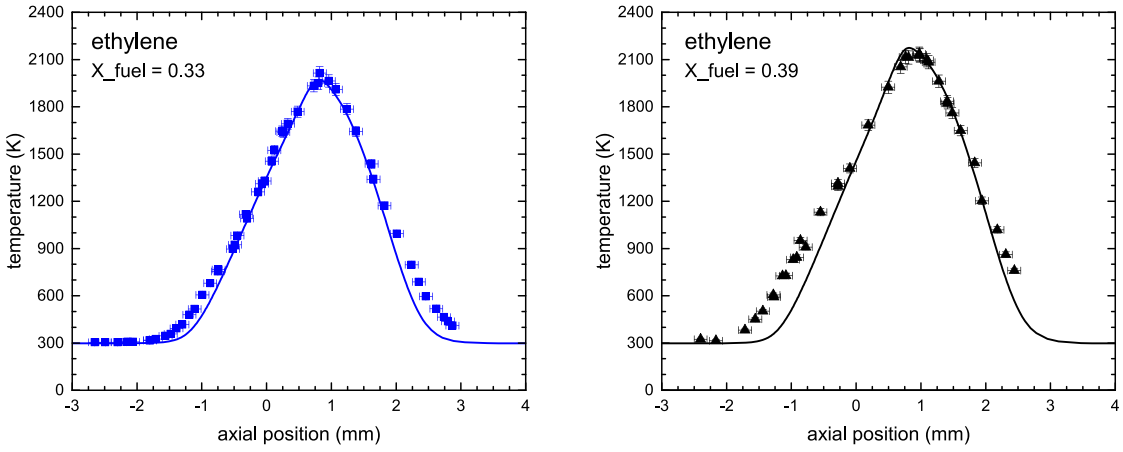

Fig. 2. Profiles of temperature for the same flame as in Fig. 1 (left panel) and for another sooting flame of ethylene with a different stoichiometry (right panel).

Table 1
Composition and velocity of the feed streams.

	Fuel stream		Oxidizer stream		T_{max}	T_{ad}
	X_F	V_{avg} (cm/s)	X_{O2}	V_{avg} (cm/s)	K	K
Methane	0.500	26.8	0.297	23.2	2158	2418
	0.530	26.9	0.321	23.1	2257	2484
	0.550	27.0	0.338	23.0	2307	2524
	0.570	27.0	0.355	23.0	2359	2561
	0.600	27.2	0.381	22.8	2429	2612
	0.650	27.4	0.428	22.6	2542	2687
	0.700	27.6	0.478	22.4	2637	2752
acetylene	0.280	25.3	0.164	24.7	1843	2134
	0.290	25.3	0.17	24.7	1892	2180
	0.300	25.3	0.176	24.7	1939	2223
	0.310	25.3	0.182	24.7	1985	2263
Ethylene	0.330	25.2	0.229	24.8	1972	2320
	0.350	25.2	0.243	24.8	2043	2382
	0.370	25.2	0.258	24.8	2110	2437
	0.390	25.2	0.272	24.8	2174	2487
	0.410	25.2	0.287	24.8	2233	2532
	0.430	25.3	0.301	24.7	2289	2573
Propene	0.280	24.4	0.256	25.6	2032	2399
	0.300	24.4	0.273	25.6	2107	2457
	0.320	24.3	0.289	25.7	2175	2508
	0.340	24.3	0.305	25.7	2238	2553
	0.350	24.3	0.313	25.7	2267	2574
Propane	0.340	24.2	0.334	25.8	2240	2558
	0.370	24.1	0.359	25.9	2322	2613
	0.400	24.0	0.384	26.0	2397	2660
	0.430	24.0	0.409	26.0	2464	2701

$Z_{st} = 0.183$ and the global strain rate $a = 50s^{-1} = (V_{avg,f} + V_{avg,ox})/L$ so that the position of the flame with respect to the gas stagnation plane and the residence time are constant. Five aliphatic fuels are tested: methane, ethylene, acetylene, propene and propane. Table 1 shows reactant mole fractions (with nitrogen as the complement to unity) and average velocities at the burner outlets, computed maximum temperature and adiabatic flame temperature for each of 26 flames.

2.2. Pyrometry

Soot volume fraction is measured via pyrometry using a Nikon D70 digital camera with a well characterized spectral response (400 nm-700 nm) as described exhaustively in past work [12,13]. Flame flickering, as determined by the position of the flame chemiluminescence, is confined to within the pixel resolution. An Abel transform deconvolves the line-of-sight images of each color channel into two-dimensional fields and the ratio of any two Abel-transformed color channels is related to the intensity of radiation emitted through Planck's law. The soot volume fraction is calculated as

$$f_v = -\frac{\lambda_e}{\tilde{K}_{ext} L_p} \ln\left\{1 - \epsilon_c(\lambda_e)\frac{\tau_c S_s}{\tau_s S_c}\exp\left[-\frac{hc}{k_B \lambda_e}\left(\frac{1}{T_c} - \frac{1}{T_s}\right)\right]\right\}, \quad (1)$$

where λ_e, L_p, τ, and $\tilde{K}_{ext}$ are the effective channel wavelength, pixel length, exposure time, and dimensionless extinction coefficient, respectively. We assume $\tilde{K}_{ext} = 5.34 \pm 2.68$, the variability of the extinction coefficient with wavelength and soot maturity is lumped as general uncertainty. Subscripts 's' and 'c' refer to measurements on soot particles and to a light calibration source, respectively.

2.3. Modeling

One-dimensional modeling of the flames is performed with ANSYS CHEMKIN-Pro [10] using the KAUST chemistry Mechanism (KM2) [17]. We account for multicomponent diffusion coefficients, thermal diffusion, and thermal radiation of CO, CO_2, H_2O, and CH_4

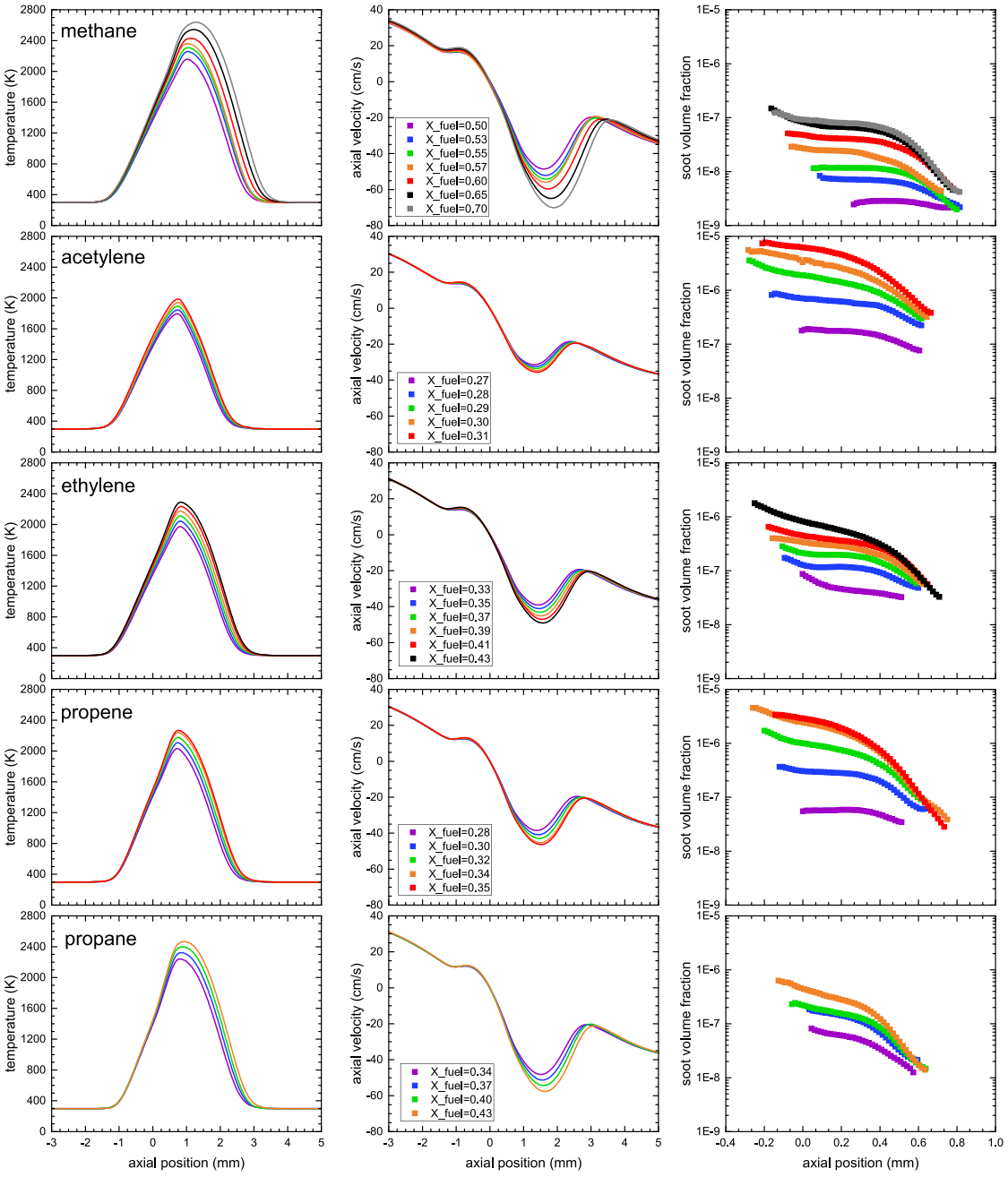

Fig. 3. Profiles of computed temperature and velocity, and of experimental soot volume fraction (left to right).

in the optically thin limit. The KM2 mechanism was validated in a baseline flame up to 6-ring PAH [14] and partially validated for surrogate mixtures [18].

3. Results and discussion

Figure 3 shows profiles of computed temperature and axial velocity component, as well as the experimental soot volume fraction. Peak temperatures, presented in Table 1, span a range that is fuel specific and is determined by ensuring that the soot load is compatible with the assumption of negligible radiative heat losses. To estimate such losses from soot, the soot volume fraction is modeled in Chemkin using an empirically derived single reaction soot model that is appended to the KM2 mechanism [19]. All investigated flames are found to have less than a 20 K reduction in temperature from soot radiation, which has no bearing on our data processing. Soot volume fraction is detected in the spatial range between 0.2 mm and 0.8 mm, with soot growing more or less monotonically (right to left) from the high temperature region on the fuel side to progressively lower and lower temperature as the particles migrate towards the particle stagnation plane past the origin of the abscissa, consistently with our previous work on counterflow diffusion flames. Soot volume fraction is lowest in the methane flames, barely reaching 10^{-7} in the hottest methane flame, and largest in the acetylene flames, reaching almost 10^{-5}, even though the peak temperature in such flames is kept below 2000 K.

We now combine the experimental soot data with the computational results for temperature and axial velocity component to quantify the soot production rate. The governing equation for

soot in an axis-symmetric flow field yields the net soot production rate, $\dot{\omega}_s$, as

$$\dot{\omega}_s''' = \frac{d}{dz}(\rho Y_s \cdot V_{ax}) + \rho Y_s \cdot \frac{d}{dr}(V_r) + \frac{d}{dz}(\rho Y_s \cdot V_{th}) + \frac{d}{dz}(\rho Y_s \cdot V_P), \tag{2}$$

where ρ, V_{ax}, and dV_r/dr are the gas density, the axial velocity and the radial derivative of the radial velocity component (i.e., local strain rate) from the one-dimensional model and the soot mass fraction $Y_s = (\rho_s f_v)/\rho$, is determined from knowledge of the local value of the gas density, ρ, from the modeling and the experimental measurements of f_v. The net soot production rate on the left hand side in principle accounts for both positive soot production, i.e. soot formation and destruction via oxidation, that is, $\dot{\omega}_s''' = \dot{\omega}_{sf}''' + \dot{\omega}_{so}'''$. However, in the present experiments soot forms on the fuel side near the flame and travels towards GSP and PSP in an environment that is free of both O_2 and OH. Hence, there is no oxidation. Therefore, $\dot{\omega}_s$represents just the positive soot production rate, that is, $\dot{\omega}_s''' = \dot{\omega}_{sf}'''$. On the righthand side of Eq. (2) one finds the convective and diffusive (transport) terms of the soot governing equations with the last two terms as the contributions due to thermophoresis and Brownian diffusion, respectively.

Integrating Eq. (2) along the transverse direction provides the soot production rate per unit flame surface area, $\dot{\Omega}_{sf}''$, as

$$\dot{\Omega}_{sf}'' = \int_{z_1}^{z_2} \dot{\omega}_{sf} dz \cong \int_{z_1}^{z_2} \left[\rho Y_s \cdot \frac{d}{dr}(V_r)\right] dz, \tag{3}$$

where all other terms from the RHS of Eq. (2) cancel out once integration is carried out over an interval whose bounds, z_1 and z_2, are outside the region along the flame axis where soot is detectable where Y_s is identically zero.

We use the approximate equality, since the last term in Eq. (3) relies on the *experimental* determination of Y_s. The evaluation of Eq. (3) for each flame is plotted in Fig. 4a versus the peak flame temperature (see Table 1). We note that each fuel correlates linearly on a logarithmic scale with the peak flame temperature. A similar result would have been obtained if we had used the adiabatic flame temperature in the abscissa. At a fixed peak flame temperature, say 2200 K soot production rate scales as propene>ethylene>propane>methane with values of 3.5 10^{-5}, 8 10^{-6}, 1.1 10^{-6}, 9 10^{-8} g/(cm^2 s), respectively, whereas acetylene shows an extrapolated value much larger than all other fuels by more than two orders of magnitude (4.0 10^3). Two remarks are in order. First, the high soot loading in acetylene flames was attributed to the inherently high temperatures of such flames in [20], notwithstanding the fact that flame dilution by nitrogen affected the sooting behavior of the flame both in terms of temperature and concentration, as pointed out in [21]. The present results show that acetylene high soot production rate is *intrinsic* of the fuel and persists even at relatively low temperatures. Second, we report methane soot production rate, which is largely due to the formation of C2 hydrocarbons in methane pyrolysis, whereas no values are reported in the literature in terms of either TSI or YSI. This finding may be useful in practical applications using natural gas of which methane is a primary constituent.

A more detailed comparison of our data with smoke height, TSI and YSI is not warranted first because there is a paucity of data on gaseous fuels, with the exception of Ref. [20] on which we already commented, and second because we would be comparing quantitative soot production rates with indirect measurements of soot propensity. Even though YSI is a semiquantitative improvement over smoke height and TSI because it measures directly the peak soot volume fraction, peak soot volume fraction and total soot

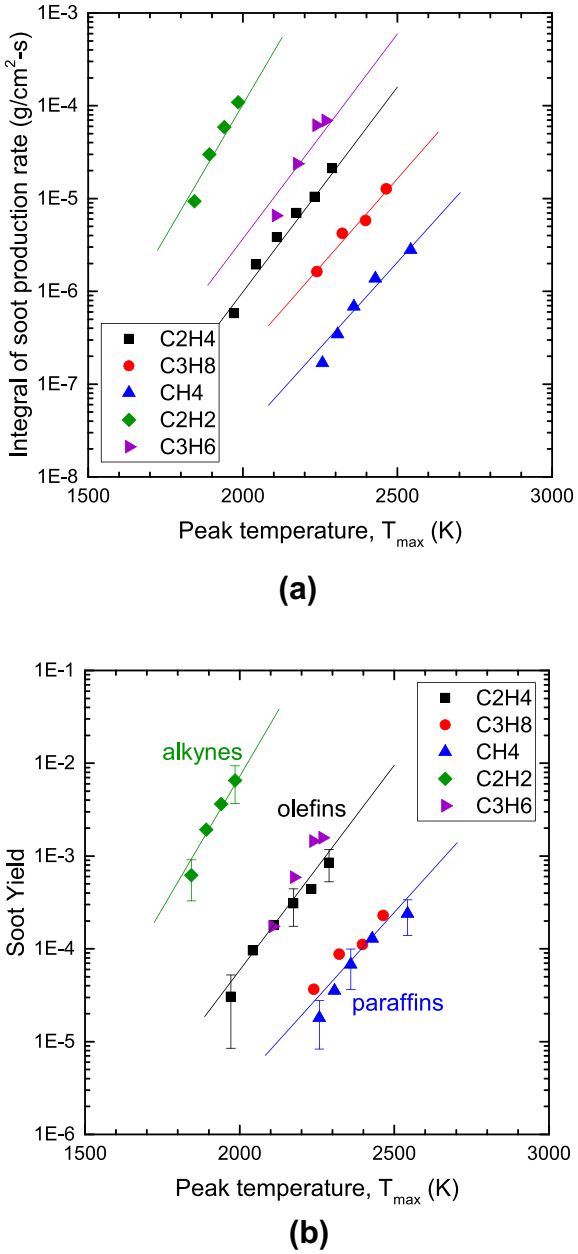

Fig. 4. Soot production rate per unit area (a) and soot yield (b) versus peak flame temperature.

production rate in a flame are not the same quantities and the latter ought to be the desired quantity to characterize the sooting behavior of fuels as derived from the soot governing equation.

Nondimensionalizing Eq. (3) as

$$\tilde{\Omega}_s = \frac{\dot{\Omega}_{sf}'' A_n}{\dot{m}_c}, \tag{4}$$

where A_n is the burner nozzle area and $\dot{m}_c$ is the carbon mass flow rate (mass flow rate multiplied by number of carbon atoms) for each flame results in the soot yield, as a function of peak temperature, as plotted in Fig. 4b. Error bars in the reported measurements include the uncertainty in measured volume fraction and carbon mass flow rate. The error in the measured volume fraction from Eq. (1), which accounts for most of the error in the soot yield, is determined by error propagation of the measured color ratio, the emissivity of the calibrating thermocouple, the measured tempera-

ture, the extinction coefficient, and an estimate of the transmission efficiency of the camera as well as the entire optical lensing system. This soot yield is a quantitative assessment representing soot production rate per flow rate of carbon atoms and revealing how much of that carbon is converted into soot. When nondimensionalized, the data cluster by fuel type with the propensity scaling as alkynes>olefins>paraffins, ranging between 10^{-2} for acetylene and 10^{-5} for paraffins. This ranking of aliphatics is in agreement with early studies in laminar diffusion flames [22,23] in contrast with those of Ref. [20].

This proof-of-concept of a simple but quantitative assessment of soot production rate is focused on gaseous fuels. Extension to other fuels, including liquids, blends and (surrogates of) practical fuels are eminently feasible by using the same doping approach implemented in the formulation of YSI [6], with the advantage that the temperature and velocity field is fixed in the baseline flame and the perturbation on these variables associated with the doping of fuels of different sooting tendencies is negligible so long as the soot loading is modest. Indeed, the doping approach was used in much of our earlier work with liquid fuels in counterflow flames [24–27].

4. Conclusions

A simple method is proposed for a direct, *quantitative* assessment of soot production rate and its temperature dependence. Testing on aliphatic fuels, including methane, propane, ethylene, propene and acetylene, in a total of 26 flames, shows that soot production rate per unit area ranges from 10^{-4} to 10^{-7} g/(cm^{2}s) and, when normalized with respect to carbon flux, from 10^{-5} to 10^{-2}. At fixed temperature it scales as alkanes< alkenes< alkynes. The production rate in a logarithmic scale correlates linearly with peak temperature for all fuels.

Novelty and significance statement

The novelty of the work is the introduction of a quantitative assessment of soot formation rate requiring a simple experimental method and the use of (open-source) computational modeling of counterflow flames.

Authors contributions

AG conceived the study, supervised the data analysis and wrote the article: KG performed the experimental work, analyzed data and edited the article.

Declaration of Competing Interest

The authors declare that they have no known competing financial interests or personal relationships that could have appeared to influence the work reported in this paper.

Acknowledgments

This article is dedicated to the late Professor Irv Glassman of Princeton University, who exposed the senior author (AG) to research on soot through smoke height measurements at the beginning of his Ph.D. thesis in the ‘80s. The quantitative alternative that is presented in this article retains the simplicity that Glassman advocated throughout his work and benefits from the progress in the computational modeling of laminar flames in the past several decades. The authors acknowledge the support of the National Science Foundation (CBET-1853150) and declare no competing interests.

References

[1] R.L. Schalla, G.E. McDonald, Variation in smoking tendency among hydrocarbons of low molecular weight, Ind. Eng. Chem. 45 (1953) 1497–1500.
[2] Y. Yang, A.L. Boehman, R.J. Santoro, A study of jet fuel sooting tendency using the threshold sooting index (TSI) model, Combust. Flame 149 (2007) 191–205.
[3] H.F. Calcote, D.M. Manos, Effect of molecular structure on incipient soot formation, Combust. Flame 49 (1983) 289–304.
[4] L. Li, P.B. Sunderland, An improved method of smoke point normalization, Combust. Sci.Technol. 184 (2012) 829–841.
[5] C.S. McEnally, L.D. Pfefferle, Improved sooting tendency measurements for aromatic hydrocarbons and their implications for naphthalene formation pathways, Combust. Flame 148 (2007) 210–222.
[6] D.D. Das, C.S. McEnally, T.A. Kwan, J.B. Zimmerman, W.J. Cannella, C.J. Mueller, L.D. Pfefferle, Sooting tendencies of diesel fuels, jet fuels, and their surrogates in diffusion flames, Fuel 197 (2017) 445–458.
[7] J. Zhu, J.V. Alegre-Requena, P. Cherry, et al., Sooting tendencies of terpenes and hydrogenated terpenes as sustainable transportation biofuels, Proc. Combust. Inst. (2022) Supplemental Materials, doi:10.1016/j.proci.2022.07.152.
[8] A. Gomez, I. Glassman, Quantitative comparison of fuel soot formation rates in laminar diffusion flames, Proc. Combust. Inst. 21 (1988) 1087–1095.
[9] Y. Wang, S.H. Chung, Soot formation in laminar counterflow flames, Prog. Energy Combust. Sci. 74 (2019) 152–238.
[10] ANSYS CHEMKIN-Pro Release R2, (2019).
[11] OpenSMOKE++, https://www.opensmokepp.polimi.it/.
[12] K. Gleason, F. Carbone, A. Gomez, Effect of temperature on soot inception in highly controlled counterflow ethylene diffusion flames, Combust. Flame 192 (2018) 283–294.
[13] K. Gleason, F. Carbone, A. Gomez, Pressure and temperature dependence of soot in highly controlled counterflow ethylene diffusion flames, Proc. Combust. Inst. 37 (2019) 2057–2064.
[14] K. Gleason, F. Carbone, A.J. Sumner, B.D. Drollette, D.L. Plata, A. Gomez, Small aromatic hydrocarbons control the onset of soot nucleation, Combust. Flame 223 (2021) 398–406.
[15] F. Carbone, F. Cattaneo, A. Gomez, Structure of incipiently sooting partially premixed ethylene counterflow flames, Combust. Flame 162 (2015) 4138–4148.
[16] L. Figura, F. Carbone, A. Gomez, Challenges and artifacts of probing high–pressure counterflow laminar diffusion flames, Proc. Combust. Inst. 35 (2015) 1871–1878.
[17] Y. Wang, A. Raj, S.H. Chung, A PAH growth mechanism and synergistic effect on PAH formation in counterflow diffusion flames, Combust. Flame 160 (2013) 1667–1676.
[18] S. Park, Y. Wang, S.H. Chung, S.M. Sarathy, Compositional effects on PAH and soot formation in counterflow diffusion flames of gasoline surrogate fuels, Combust. Flame 178 (2017) 46–60.
[19] K. Gleason, Soot formation in high-pressure counterflow flames Ph.D Thesis, Yale University, 2020.
[20] I. Glassman, P. Yaccarino, The temperature effect in sooting diffusion flames, Proc. Combust. Inst. 18 (1981) 1175–1183.
[21] R.L. Axelbaum, W.L. Flower, C.K. Law, Dilution and temperature effects of inert addition on soot formation in counterflow diffusion flames, Comb. Sci. and Tech 61 (1988) 51–73.
[22] A.E. Clarke, T.G. Hunter, F.H. Garner, The tendency to smoke of organic substances on burning, J. Inst. Pet. Technol. 32 (1946) 627–642.
[23] R. Hunt, Relation of smoke point to molecular structure, Ind. Eng. Chem. 45 (1953) 602–606.
[24] S. Jahangirian, C.S. McEnally, A. Gomez, Experimental study of ethylene counterflow diffusion flames perturbed by trace amounts of jet fuel and jet fuel surrogates under incipiently sooting conditions, Combust. Flame 156 (2009) 1799–1809.
[25] F. Carbone, A. Gomez, The structure of toluene-doped counterflow gaseous diffusion flames, Combust. Flame 159 (2012) 3040–3055.
[26] F. Carbone, A. Gomez, Chemical effects of 1,2,4-trimethyl benzene addition in counterflow gaseous diffusion flames, Proc. Combust. Inst. 34 (2013) 1025–1033.
[27] K. Gleason, A. Gomez, Detailed study of the formation of soot precursors and soot in highly controlled ethylene(/toluene) counterflow diffusion flames, J. Phys. Chem. A 127 (2023) 276–285.